CHAPTER 3

Electrical Resistivity Surveys

This chapter includes fundamental principle of electrical resistivity surveying method and application of 3D electrical resistivity techniques to the Intakhin kilns site. The 3D electrical resistivity data were processed using RES3DINV inversion program with smoothness-constrained algorithms. The 3D electrical resistivity inversion results revealed information about the kilns structures located near to the surface.

3.1 Resistivity Method

Resistivity surveying on archaeological sites indicate spatial differences in sediment moisture. The presence of features, architecture, activity areas, and other archaeological remains can be detected if the amount of moisture they retain is different from that retained by surrounding sediment. The location of these anomalies or contrasts involves careful measurement of the sediment resistivity at discrete points on the surface along traverses, or on a grid of points (Tagg, 1964).

3.1.1 Geo-Electrical Resistivity

In order to successfully conduct and interpret a resistivity survey, a grasp of basic electrical theory is necessary, beginning with the nomenclature. Electric current is defined as the rate of flow of charge passing through a cross section of a conducting medium for a specific length of time (Marescot, 2006). To cause charge to flow, a voltage must first be applied. When a voltage is applied and a current flows, a resistance is encountered within the movement of the charge, which is dependent upon the characteristics of the medium in which the charge is moving. These three physical quantities are related to Ohm's law (Telford et al., 1990), wherein,

$$R = \frac{V}{I} \tag{3.1}$$

Resistance (R) is measured in Ohms (Ω), voltage (V) in volts (V), and current (I) in amperes (A).

The current as a quantity is moved, and the resistance is the opposition encountered by moving the current. From Ohm's law, the concept of resistivity is incorporated into (3.1) the geometry of the medium.

Resistivity is a more useful quantity than resistance, in the examination aims of archaeological sites, because of the specifics of the medium and the independence of the geometry of the material being surveyed (Tagg, 1964). Resistivity (ρ) is defined as,

$$\rho = \frac{V/L}{J} \tag{3.2}$$

where, *V/L* is the change of voltage with distance in the direction of current flow, and *J* is the current density in the medium within which the charge is flowing.

The basic unit of resistivity is the ohm-meter (Ω.m), and the inverse of resistivity is known as 'conductivity' (Resnick and Halliday, 1966).

3.1.2 Electrical Properties of Soil Sediments

Sediments of soil profiles have developed rapidly and are considered through resistivity measurements that may be measured in other sedimentary types (sand, till, mud, and so forth).

The conduction of current in soils is largely an electrolytic phenomenon, that is, moisture in a soil containing freely charged particles being responsible for current flow. The resistance to currents flowing in all soil types depends upon such variables (Tagg, 1964).

Soil moisture content, which at archaeologically significant depths is generated by rainfall, occasionally entertains contributions from area having high water tables or from nearby streams. The amount of water that such soil can contain is determined by

soil porosity, which exhibits wide spatial variations according to soil type, shapes of the constituent grains, and its amount of compaction (Al Chalabi and Rees, 1962).

When considering permeability, although some soil might have a high water content, current cannot flow unless connections exist between its interstitial pores.

With regards to ion content, ions are responsible for conduction in the soil which come from dissolved salts, such as calcium and sodium carbonates. It may be derived from a variety of cultural and non-cultural sources from the soil, geologic strata, rainwater, agricultural fertilizers or compounds, by cultural processes (Tagg, 1964).

3.1.3 Soil Resistivity

Differences in soil moisture, dissolved salts, and like factors are also responsible for producing culturally formed resistivity contrasts that are detected at archaeological sites (Tagg, 1964). The values of resistivity differ in soils, as seen in Table 3.1 (Tagg, 1964).

Table 3.1 Values of resistivity differ in soils (Modified from Tagg, 1964).

Type of Soil	Resistivity (Ohm.m)
Clays	8 - 50
Loams	5 - 50
Laterites	25 - 1500

Although conduction of current in soils and archaeological sites are understood fairly well, one cannot easily predict which archaeological features will be detectable by resistivity surveying, or whether soil noise will confuse or mask cultural resistivity contrasts, because the state of the physical remains depends upon environmental and cultural history, and a feature which is easily located by resistivity surveying in one area may be imperceptible in another.

3.1.4 Electrical Resistivity Measurement

Electrical resistivity measuring is the distribution of electrical potential in the ground of an electrode array which measures the electrical resistivity distribution of the surrounding soils and rocks (Figure 3.1) (Chambers et al., 1999).

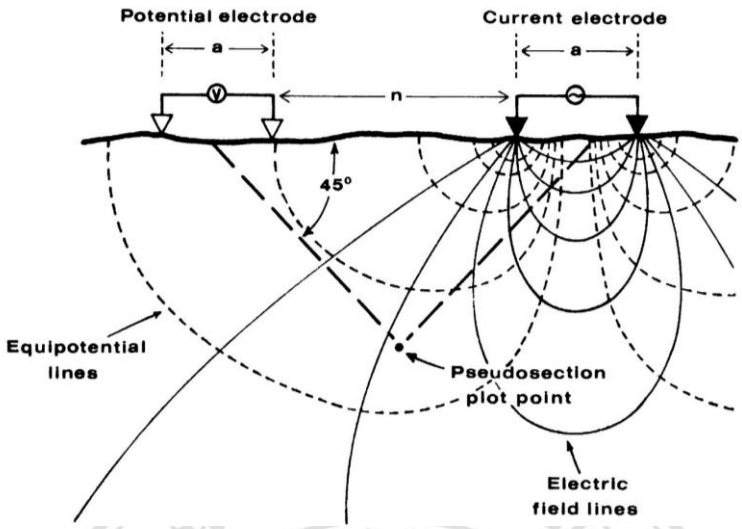

Figure 3.1 Arrangements of 4 electrodes spreads show a current flow in resistivity survey (From Chambers et al., 1999).

The potential difference (ΔV) between potential electrodes (P_1 and P_2) comes from injecting a direct electrical current through 2 electrodes (C_1 and C_2) implanted in the ground. This can be represented by Figure 3.2 (Telford et al., 1990). The potential difference can be expressed as

$$\Delta V = \frac{I\rho}{2\pi}\left\{\left(\frac{1}{r_1}-\frac{1}{r_2}\right)-\left(\frac{1}{r_3}-\frac{1}{r_4}\right)\right\} \tag{3.3}$$

Where , r_1 is the distance between electrode C_1 to P_1

r_2 is the distance between electrode P_1 to C_1

r_3 is the distance between electrode C_1 to P_2

r_4 is the distance between electrode P_2 to C_2

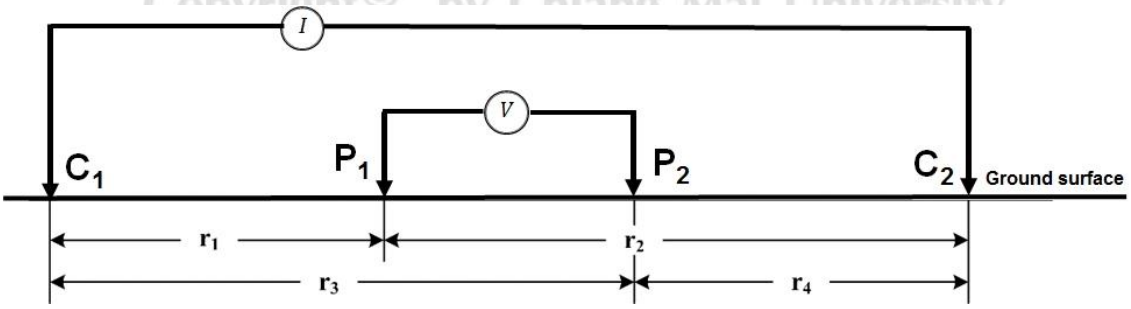

Figure 3.2 Representative electrode arrangements for four-electrode spreads commonly used in resistivity field work. (Modified from Telford et al., 1990).

3.1.5 Dipole-Dipole Array

This study is to detected kilns and archeology and therefore a dipole-dipole array is applied to this study because this array is the best for horizontal and vertical resistivity change (Mohamed Ali et al., 2007).

It is applicable to acquire data of different depths along the profiles. The convention for a dipole-dipole array is that current and voltage spacing is the same a, and the spacing between them is an integer multiple of a and na (Figure 3.3) (Loke, 2001).

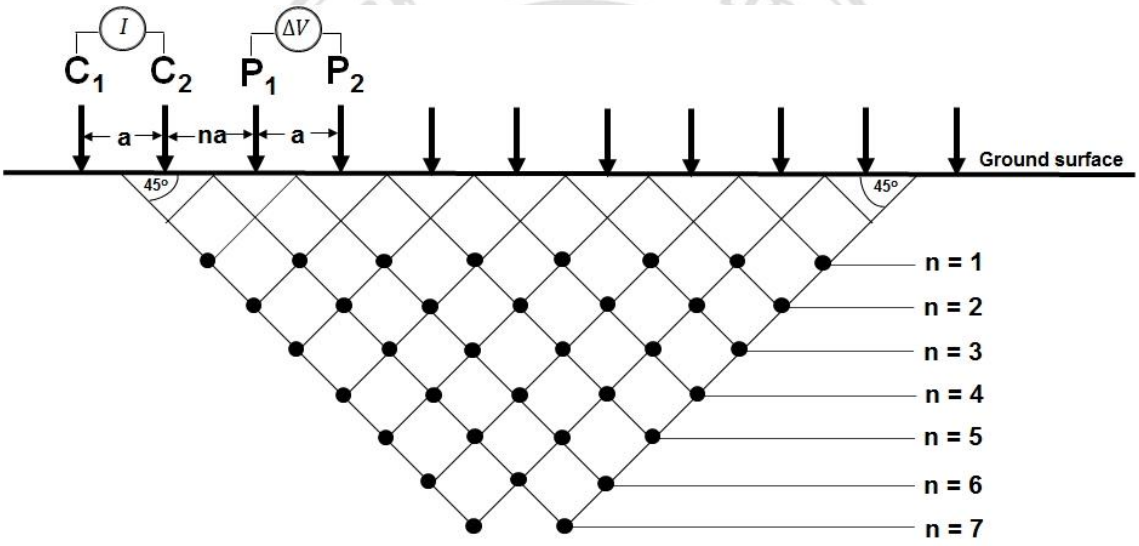

Figure 3.3 Datum point of a dipole-dipole array (Modified from Loke, 2001).

The point of apparent resistivity value is at the intersection point of two 45° lines descending from the current dipole and from the voltage dipole. The apparent resistivity of the dipole-dipole array (Telford et al., 1990) is given by

$$\rho_a = K\frac{V}{I} \tag{3.4}$$

When, $$K = \pi n(n+1)(n+2)a \tag{3.5}$$

Where, K is array geometric factor.

3.1.6 3D Resistivity Surveying

The dipole-dipole arrays in 3D electrical resistivity surveys have been reported by square and rectangle grids of electrodes, with constant electrode spacing in both x and y directions (Figure 3.4), in which each electrode is in turn used as the current electrode and the potential measured at all electrode positions were used (Loke and Barker, 1996).

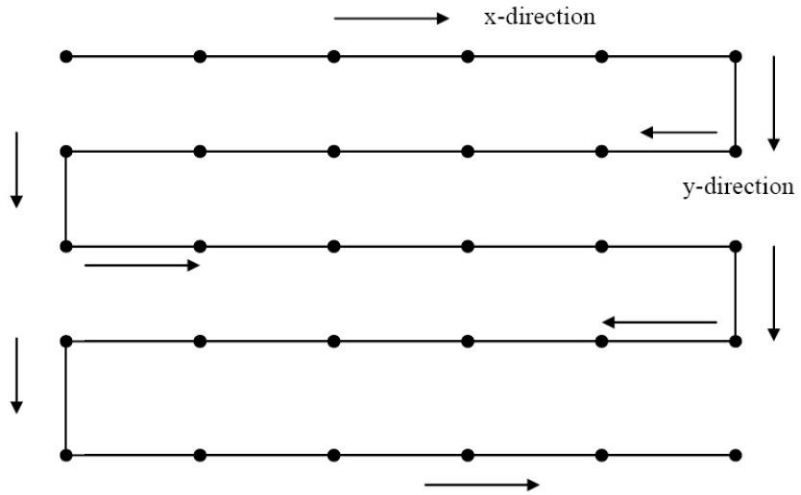

Figure 3.4 The arrangement of electrodes for a grid in 3D resistivity survey (From Loke and Barker, 1996).

The 3D data measurements sets using the square or rectangle grids of electrodes is consuming and cumbersome in surveys involving large grids, and the number of possible electrodes for the measurements is very large. To reduce the number of measurements and time required to carry out a 3D resistivity survey, this study proposed a cross-diagonal survey method in which potential measurements were only made at the electrodes along the x-axis, y-axis, and 45-degree diagonal lines passing through the current electrodes (Loke and Barker, 1996), as seen in Figure 3.5

a) Survey to measure the complete data set b) Cross-diagonal survey

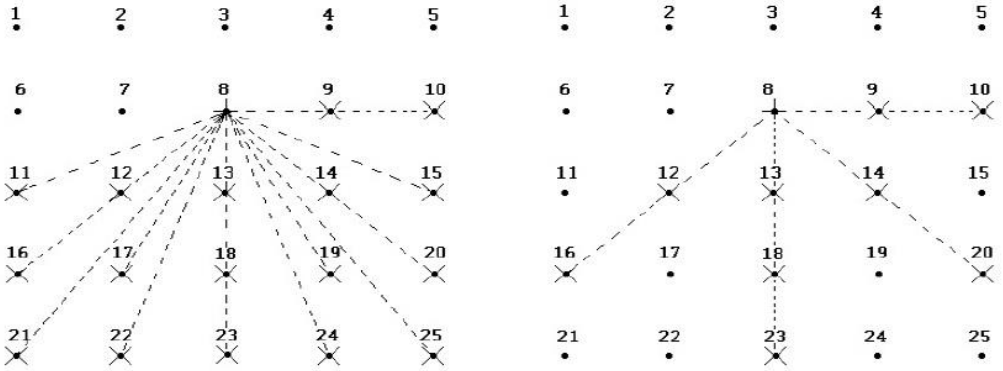

+ Current electrode × Potential electrode

Figure 3.5 Two possible measurement sequences for a 3D electrical resistivity survey use potential electrodes corresponding to a single current electrode in (a) a complete data set survey, and (b) a cross-diagonal survey (From Loke and Barker, 1996).

3.1.7 Theoretical 3D Inversion

The inversion routine used by RES3DINV is based upon the smoothness constrained least-squares method (deGroot-Hedlin and Constable, 1990, Loke et al., 2003). The basic smoothness-constrained least-squares method is based upon the following (3.6)

$$(J^T J + \lambda F)\Delta q_k = J^T g - \lambda F q_k \quad (3.6)$$

Where, $F = \alpha_x C_x^T C_x + \alpha_y C_y^T C_y + \alpha_z C_z^T C_z$

C_x, C_y= horizontal roughness filters

C_z = vertical roughness filter

$\alpha_x, \alpha_y, \alpha_z$ = relative weights in x-, y- and z- direction

J = Jacobian matrix of partial derivatives

J^T = transpose of J

λ = damping factor

q = model perturbation vector

g = data misfit vector

One model used to interpret the 3-D data set is shown in Figure 3.6(a). The subsurface is divided into several layers, and each layer is further subdivided into rectangles cells. Two other models that can be used are shown in Figures 3.6b and 3.6c. The second inversion model subdivides the top few layers vertically, as well as horizontally by half. Another subdivides the top few layers by half, but only in the horizontal direction (Figure 3.6c) (Loke and Dahlin 2002)

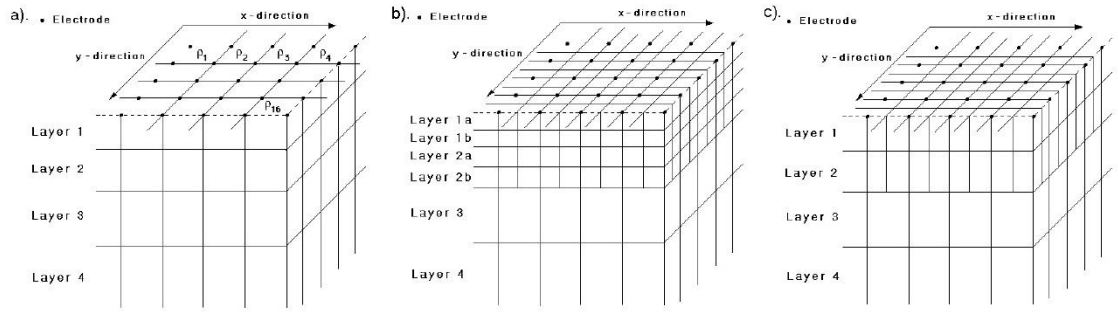

Figure 3.6 The models used in 3-D inversion (a) Standard model where the widths of the rectangles cells are equal to the unit electrode spacing in the x- and y-directions, (b) A model where the top few layers are divided by half, both vertically and horizontally, to provide better resolution, and (c) A model where the model cells are divided in the horizontal direction, but not in the vertical direction (From Loke and Barker, 1996).

This program attempts to determine the resistivity of the cells in the inversion model that will most closely reproduce the measured apparent resistivity values from the field survey. The optimization method tries to reduce the difference between the calculated and measured apparent resistivity values by adjusting the resistivity of the model blocks. A measure of this difference is given by the root-mean-square (RMS) error. However the model with the lowest possible RMS error can sometimes show large and unrealistic variations in the model resistivity values, and may not always be the 'best' model from a geological perspective (Loke and Dahlin 2002).

3.2 Resistivity Data Acquisition

Resistivity imaging surveys were carried out using a WDA-1 Super Digital DC Resistivity/IP Meter (Figures 3.7 (a) and (b)). The typical setup for 3D resistivity imaging consisted of electrodes attached to a multi-core cable. The WDA-1 resistivity

system is mainly used for electrical mapping, because this measurements is much easier and more effective.

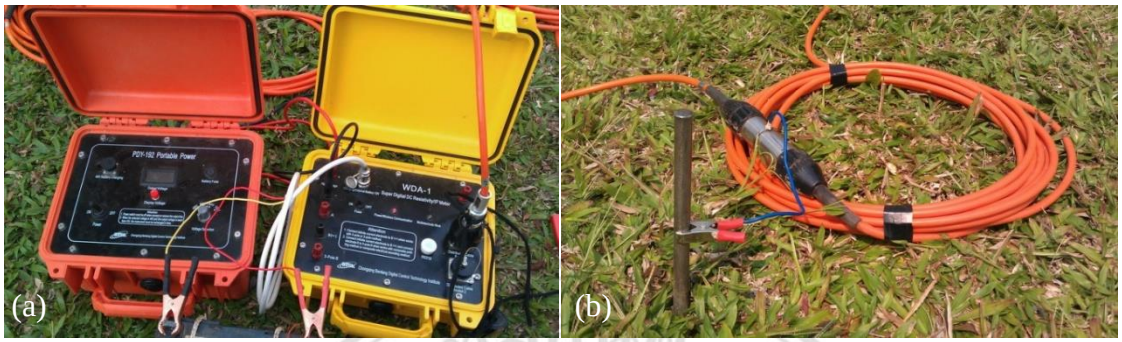

Figure 3.7 Instruments for resistivity investigation (a) WDA-1 Super Digital DC-Resistivity Meter, (b) multi-core cable and electrode.

The study area was divided into 2 search areas which covered 5 × 20 m^2, and the survey area was divided into 2 grid surveys for 1 area. Area 1 was located in the southeast of the Inthakin kiln site (Figure 1.5), and Area 2 was located in the northwest of the Inthakin kiln site (Figure 1.6).

The resistivity measurements were performed using configuration with 3D dipole-dipole having an 11x6 per grid survey (x – y direction), spacing of electrode at 1 m, and the distance between parallel lines was 1 m (Figures 3.8 - 3.9). The data set measurements used 570 data points per grid.

Figure 3.8 Layout of line survey in Area 1.

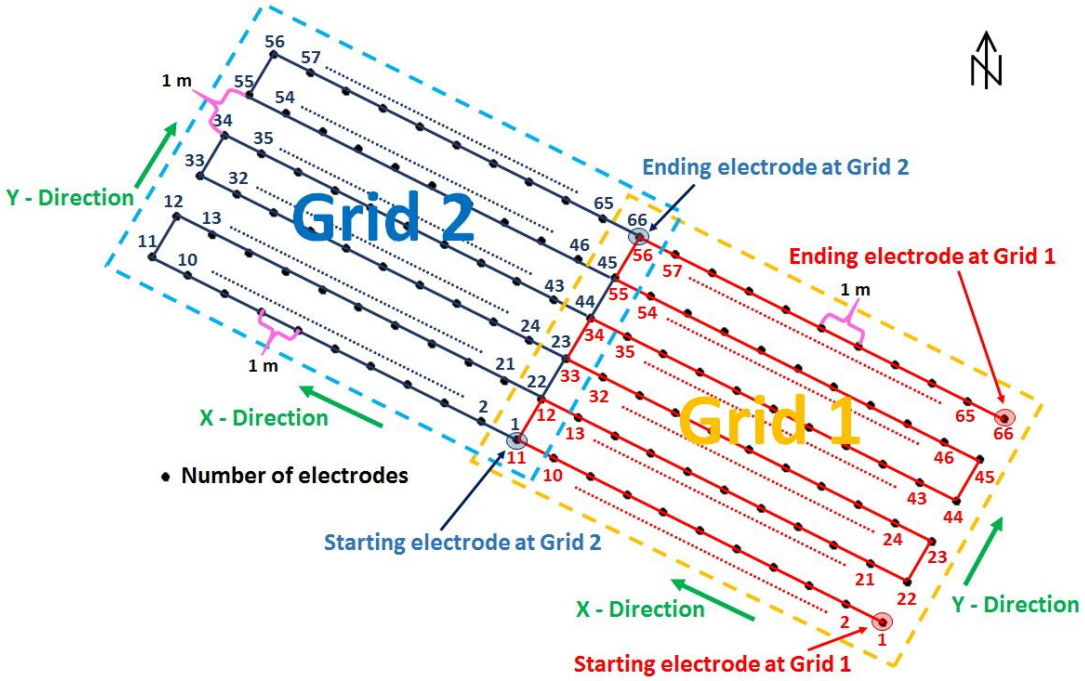

Figure 3.9 The layout of the 3D resistivity imaging at the Intakhin kiln site.

3.2.1 Limitations of the 3D Resistivity Cross-Diagonal Method

The both of study areas was divided into 2 grid surveys, covering 5 × 20 m^2. The layout of electrodes used the 3D resistivity cross-diagonal method (Figure 3.9). Datum points between grids 1 and 2 could not be collected (red zone) (Figure 3.10).

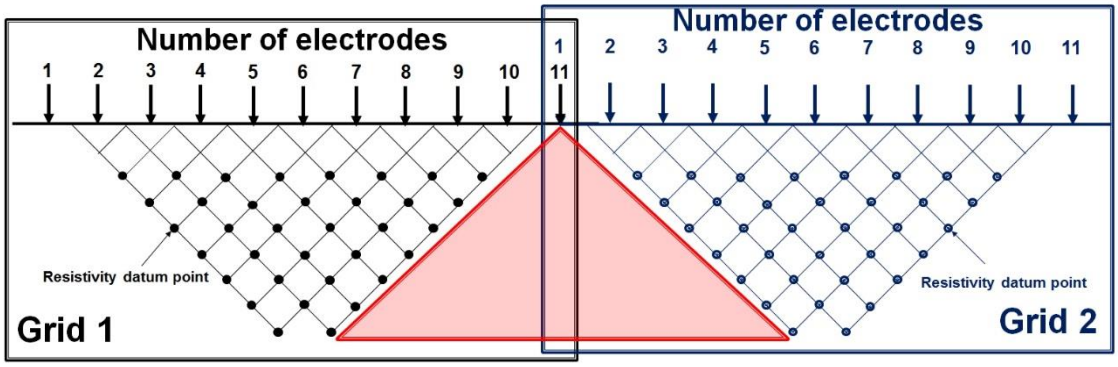

Figure 3.10 Datum points of a dipole-dipole array for 2 grids.

The resistivity inversion model in cross-sectional view shows discontinuous resistivity values (red triangle) (Figure 3.11). This in part caused greater RMS error, and thus having to be careful about interpretation of the data on this zone.

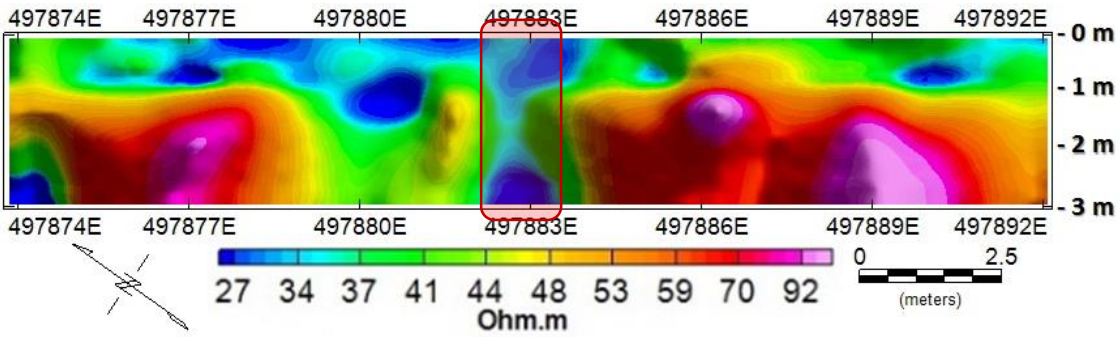

Figure 3.11 Example of 3D Inversion model of vertical slices of Area 1, Section 1.

Recommendations include the avoidance of not being able to collect data by layout roll-along electrodes, which creates continuous data.

3.2.2 Regularization Choosing Beta

The optimization explained relative emphasis on $\emptyset_m(m)$ or $\emptyset_d(m)$ in the optimization $\emptyset = \emptyset_d + \beta\emptyset_m$. It was discussed about 4 ways of specifying how β should be chosen (UBC Geophysical Inversion Facility, 2005).

- Errors in Data

Before the processing step was chosen it was necessary to make an estimate of the uncertainty of the datum, or else the inversion would not know how well that datum should be reproduced. The data reliability (date error) involved 3 concepts (UBC Geophysical Inversion Facility, 2005)

- Errors constant from all data.
- Error percentage of data.
- Error of combination were used.

Chifact, GCV or L-Curve methods may help, if the reliability of data is poor.

- Chifact

Chifact determines the value of β which is a random optimal model based upon the presumption of noise and error in the data. It behaves according to a Gaussian distribution. The misfit function $\emptyset_d(m)$ have an expected value = N (the number of

data). The inversion tries to arrange the β values, then choose a model of inversion which uses β value yielding $\emptyset_d(m) = \emptyset_d^* = N$. This is reminiscent of the Tikhonov curve (UBC Geophysical Inversion Facility, 2005).

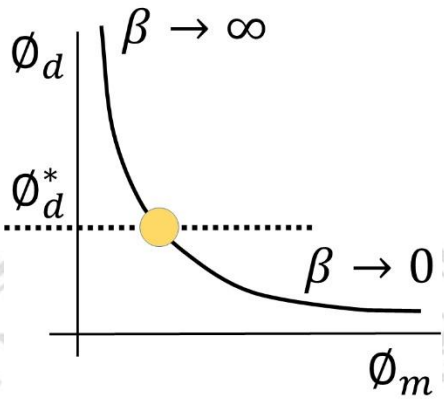

Figure 3.12 Tikhonov curve (Modified From UBC Geophysical Inversion Facility, 2005).

- Generalized Cross Validation (GCV)

The Generalized Cross Validation access β when datum errors are poor, and is attractive because it offers strong opinions to consider each data point. The opinion is used in applied mathematics including inversion, and it involves very intensive computing, many more times than when using Chifact to determine β (UBC Geophysical Inversion Facility, 2005).

- L-norm

To select β using the L-curve approach to generated range of β values, the resulting set of $\emptyset_d(m)$ and $\emptyset_m(m)$ values are plotted to create a Tikhonov curve (Figure 3.12). Using a log-log axis is called the 'L-curve'. If information is lacking in data errors, then the optimal choice for β is made by value generation of $\emptyset_d(m)$ and $\emptyset_m(m)$, braced at the point of maximum curvature on this curve (Figure 3.12). The model corresponding to specific solutions is then transformed into inversion results (UBC Geophysical Inversion Facility, 2005).

3.3 Resistivity Data Processing

Resistivity data were inverted using RES3DINV. This inversion program uses a block model in which resistivity values are assigned within the prisms of a 3D mesh (Tsourlos and Ogilvy, 1999) (Figure 3.13).

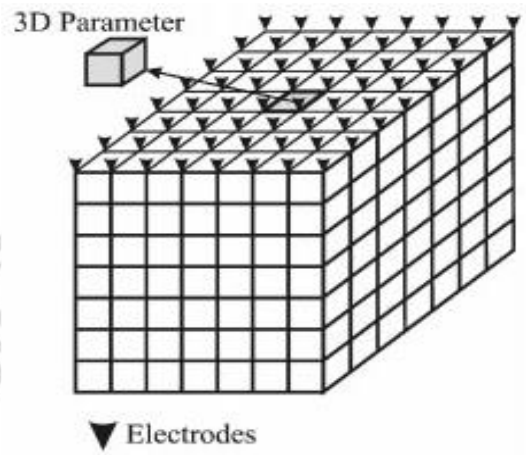

Figure 3.13 The 3D hexahedral elements to discretize the domain (From Tsourlos and Ogilvy, 1999).

The program attempts to achieve convergence between apparent resistivity values and the calculated model by using the smoothness constrained least square method (Loke and Barker, 1996) (Figure 3.14).

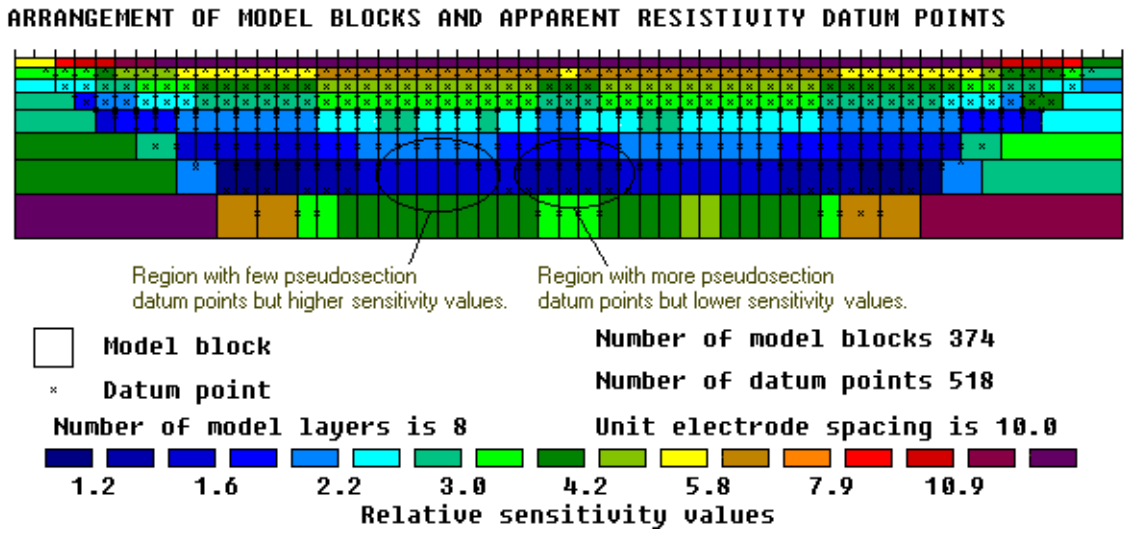

Figure 3.14 Mapping of values of the model cells used by the inversion program (From Loke and Barker, 1996).

Smoothness-constrained least square (L2 norm) is a widespread method used between regularized optimization methods. The aim of this method is to minimize the sum of squares of the spatial changes in the data misfit and model resistivity (deGroot-Hedlin and Constable, 1990).

3.3.1 Inversion Param for 3D Resistivity Processing

The inversion param used for this study are listed in Table 3.2. The initial damping factor normally has a value of between 0.05 - 0.25, with retain progressively reduced with each iteration in order to avoid instability in the model values and a larger damping factor for a noisy data set.

- The initial damping factor used was 0.15 because the data set was not noisy.
- The minimum damping factors was 0.01
- Number of iterations was 6.
- The convergence limit of 5 % was applied sets of data misfit in the inversion of the apparent resistivity data where the program would stop.
- The vertical to horizontal flatness filter ratio was 0.5, to provide information about the model emphasized in the horizontal.
- The number of nodes was 4, to add to the model grid lines in the display, and to optimize the model grid to achieve a balance between a sufficiently fine mesh and a minimum number of model cells.
- Reducing the effect of side blocks was employed to reduce causes of sensitivity values associated with the side blocks to be much larger than the neighboring interior blocks.
- Least-squares method would attempt to minimize the square of differences between the measured and calculated apparent resistivity values.
- Standard Gauss-Newton method was used to solve the least-squares equation, where an exact solution was obtained, and to make more accurate results and increases with the cube of the number of model blocks.
- Finite-difference method was not calculated in the topographical model.

Table 3.2 Inversion setting param used in the RES3DINV software.

Processing model	Parameter setting
Initial damping factors	0.15
Minimum damping factors	0.1
Number of iterations	6
Convergence limit	5 %
Vertical to horizontal flatness filter ratio	0.5
Number of nodes	4
Reduced effect of side blocks	Yes
The least-squares method	Yes
The standard Gauss-Newton method	Yes
The finite-difference method	Yes

3.4 Resistivity Data

3.4.1. 3D Resistivity Block Model

The 3D resistivity survey data were used for computing the 3D model block and the distribution was colored. For Area 1 (Figure 3.15), the model presents a logarithmic scale from 27 – 92 Ohm.m, and for Area 2 (Figure 3.16), the model presents a logarithmic scale from 94 – 336 Ohm.m. Thus, both areas contain between 20 m east, 6 m north and depths from the ground were 3 m.

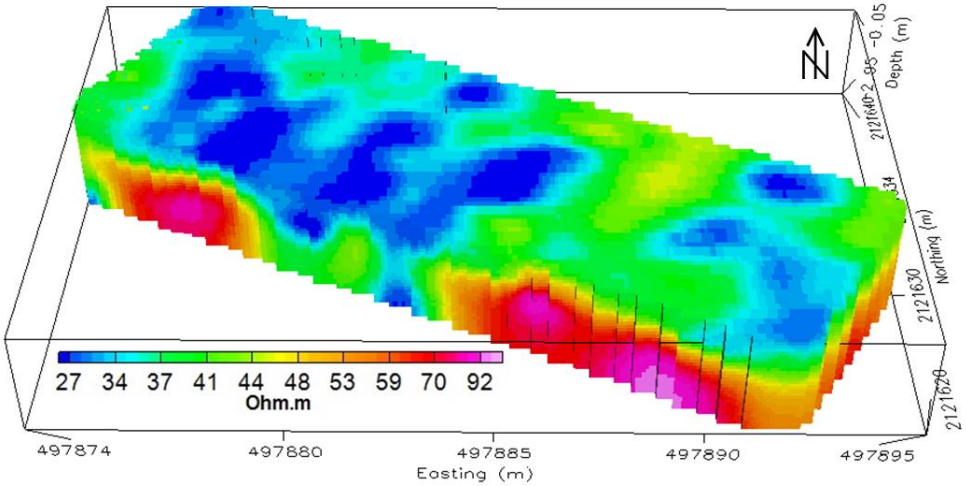

Figure 3.15 3D resistivity block model in Area 1.

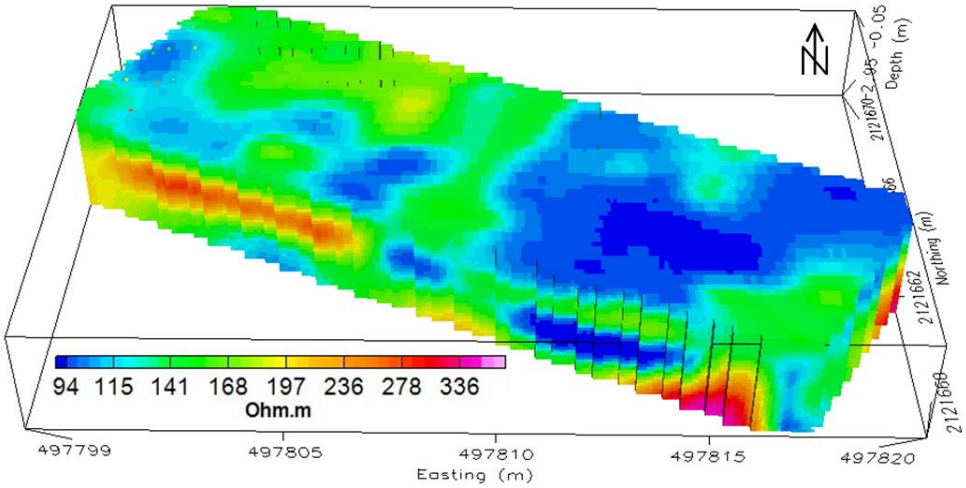

Figure 3.16 3D resistivity block model in Area 2.

3.4.2 Resistivity Depth Slice Results

From the 3D resistivity block model inversion results (Figures 3.15 – 3.16), these were divided into horizontal slices for 7 different depths in order to determine the value and appearance of any anomaly. The values of the anomalies were quite high, and similar in size to the kilns, which measured approximately 2x3 m.

Note that due to the limitations of data coverage (read in section 2.3.1) in the middle of the survey areas (Figures 3.17 – 3.18), interpretation of the resistivity data has to be aware of.

Area 1

The data acquired were inverted using RES3DINV to obtain depth slices for depths ranging from 0.1, 0.5, 1.0, 1.5, 2.0, 2.5 and 2.9 m, respectively, for horizontal in X-Y planes, using 1 m electrode spacing (Figures 3.17(a) – 3.17(g)).

For the first layer (Figure 3.17(a)), the depths of 0.1 m resistivity values ranged from 20 to 120 Ohm.m.

The second and third layer (Figures 3.17(b) - 3.17(c)), had a depth of 0.5 m, and low resistivity zone of 20 - 40 Ohm.m (blue and green). The high resistivity zone of 50 - 100 Ohm.m (orange and red), in the black rectangles, had interesting anomalies.

The fourth and fifth layers (Figures 3.17(d) – 3.17(e)), had depths of 1.5 m and 2.0 m, and low resistivity zone of 20 - 40 Ohm.m (blue and green). The high resistivity zone of 50 - 100 Ohm.m (orange and red), also in the black rectangles, also had interesting anomalies.

The resistivity of the sixth and seventh layers (Figures 3.17(f) – 3.17(g)), was at depths of 2.5 m and 2.9 m. The high resistivity values and resistivity contrasted and also had interesting anomalies.

Area 2

The data acquired were inverted using RES3DINV to obtain depth slices for depths ranging from 0.1, 0.5, 1.0, 1.5, 2.0, 2.5 and 2.9 m, respectively, for the horizontal in X-Y planes, using 1 m electrode spacing (Figures 3.18(a) – 3.18(g)).

The first layer (Figure 3.18(a)), with a depth of 0.1 m resistivity, had values ranging from 90 to 350 Ohm.m.

The second and third layer (Figures 3.18(b) - 3.18(c)) had a depth of 0.5 m and low resistivity zone of 90 - 170 Ohm.m (blue and green). The high resistivity zone was 250 - 300 Ohm.m (orange and red), in the black rectangles, had interesting anomalies.

The fourth and fifth layers (Figures 3.18(d) – 3.18(e)), of depths 1.5 m and 2.0 m, had a low resistivity zone of 90 - 170 Ohm.m (blue and green). The high resistivity zone was 250 - 300 Ohm.m (orange and red), again in the black rectangles, also had interesting anomalies.

The resistivity of the sixth and seventh layers (Figures 3.18(f) – 3.18(g)), at depths of 2.5 m and 2.9 m, had resistivity values ranging from 250 to 300 Ohm.m. The high resistivity values and resistivity contrast also had interesting anomalies.

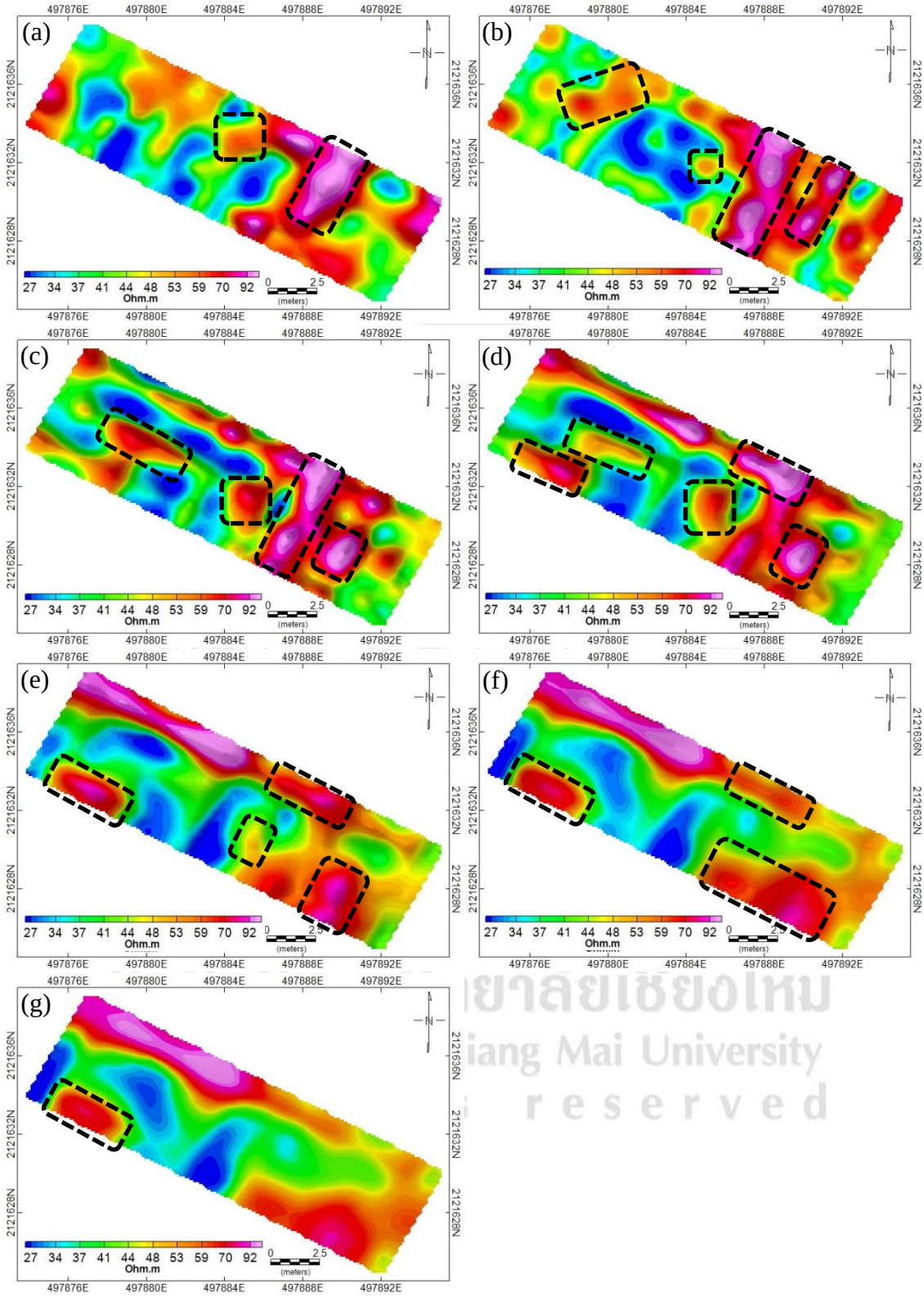

Figure 3.17 Resistivity data depth slides (X-Y plane) in Area 1 (a) 0.1, (b) 0.5, (c) 1.0, (d) 1.5, (e) 2.0, (f) 2.5 and (g) 2.9 m (The black rectangles present high resistivity anomaly zones).

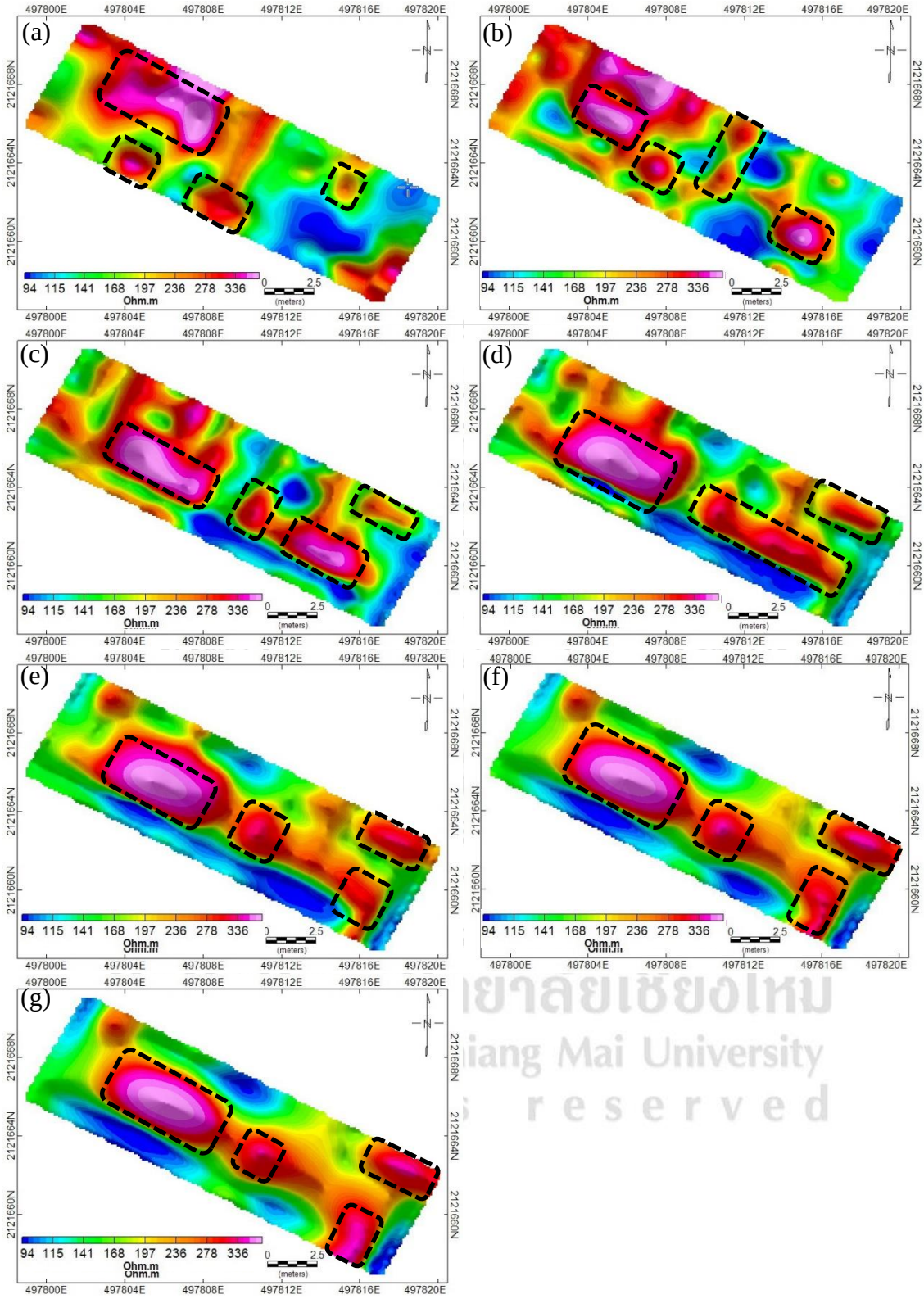

Figure 3.18 Resistivity data depth slides (X-Y plane) in Area 2 (a) 0.1, (b) 0.5, (c) 1.0, (d) 1.5, (e) 2.0, (f) 2.5 and (g) 2.9 m (The black rectangles present high resistivity anomaly zones).

The inversion results were divided into vertical slices for 5 sections in both areas to determine the value and appearance of any anomaly. The values of the anomalies of interest were quite high and similar in size to the kilns, which measured approximately 2x3 m.

3.4.3 Resistivity Vertical Slice Results

Area 1

The data inversion obtained vertical slices (section) for X-Z plane of Area 1 (Figure 3.19). The results show interesting trend of anomaly at the top and bottom of each section. The main anomalies of interest had an apparent resistivity over 50 Ohm.m, a dimension of 2x3 m, and the thickness of anomalies were 1-1.5 m and of contiguous section.

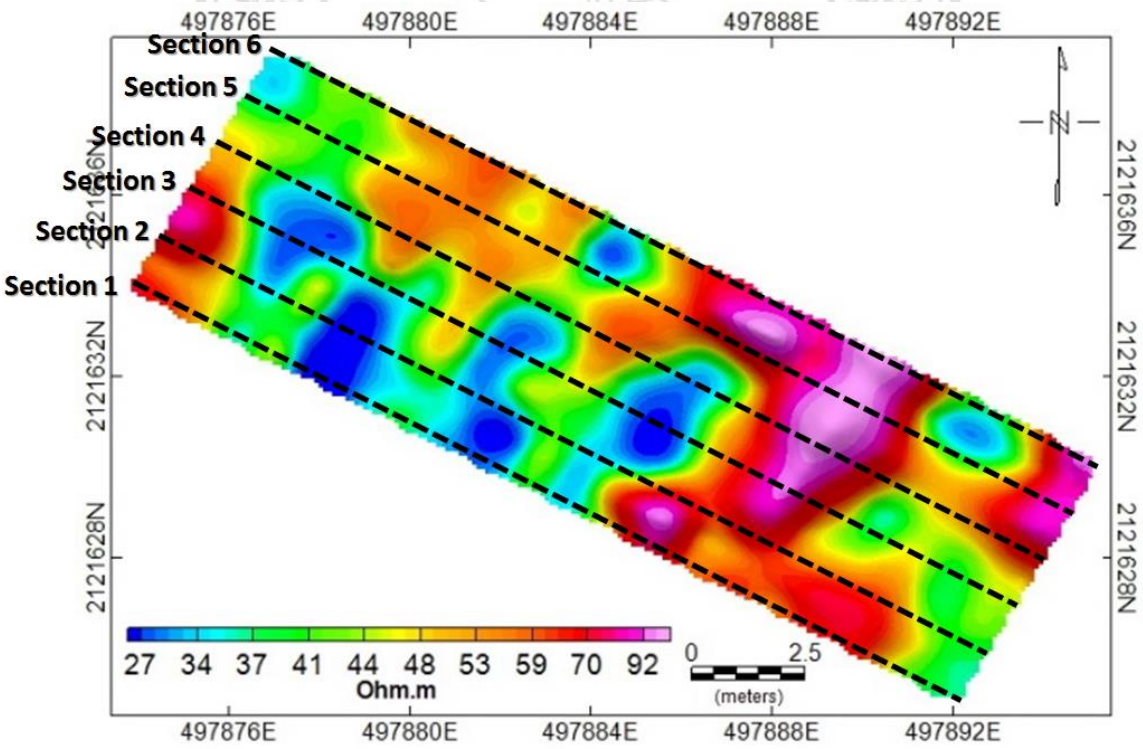

Figure 3.19 Map showing line sections of Area 1 (Dash lines are study line)

Note that due to the limitations of data coverage (read in section 2.3.1) in the middle of the survey areas (Figures 3.20 – 3.32), interpretation of the resistivity data has to be aware of.

The results of the 3D inversion model of Area 1 (Figure 3.20) shown in X-Z plane, Section 1. The anomalies of interest were in the black rectangles.

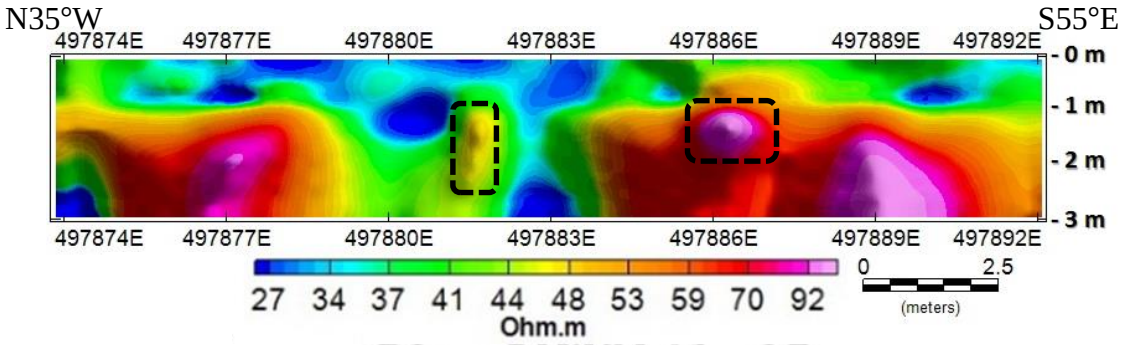

Figure 3.20 3D Inversion model of vertical slices of Area 1, Section 1 (The black rectangles present high resistivity anomaly zones).

The results of the 3D inversion model of Area 1 (Figure 3.21) shown in X-Z plane, Section 2. The anomalies of interest were in the black rectangles.

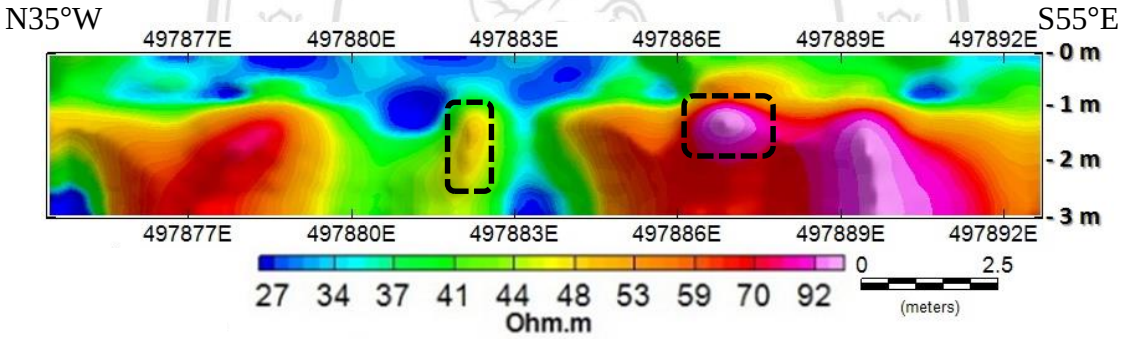

Figure 3.21 3D Inversion model of vertical slices of Area 1, Section 2 (The black rectangles present high resistivity anomaly zones).

The results of the 3D inversion model of Area 1 (Figure 3.22) shown in X-Z plane, Section 3. The anomalies of interest were in the black rectangles.

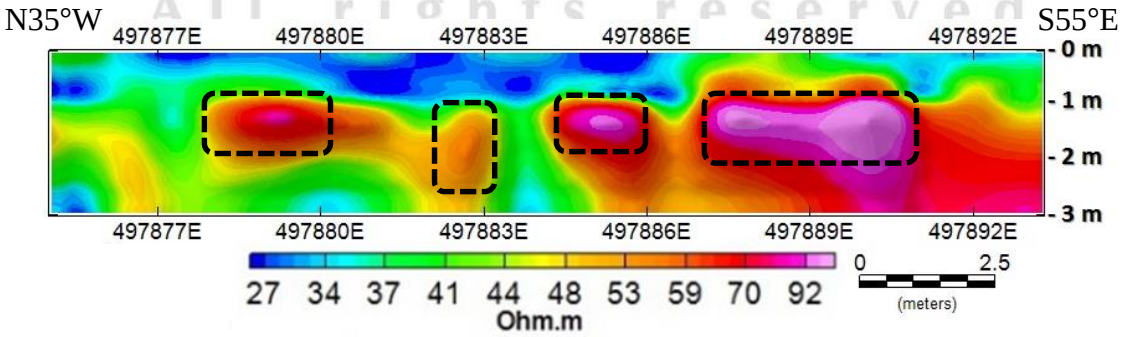

Figure 3.22 3D Inversion model of vertical slices of Area 1, Section 3 (The black rectangles present high resistivity anomaly zones).

The results of the 3D inversion model of Area 1 (Figure 3.23) shown in X-Z plane, Section 4. The anomalies of interest were in the black rectangles.

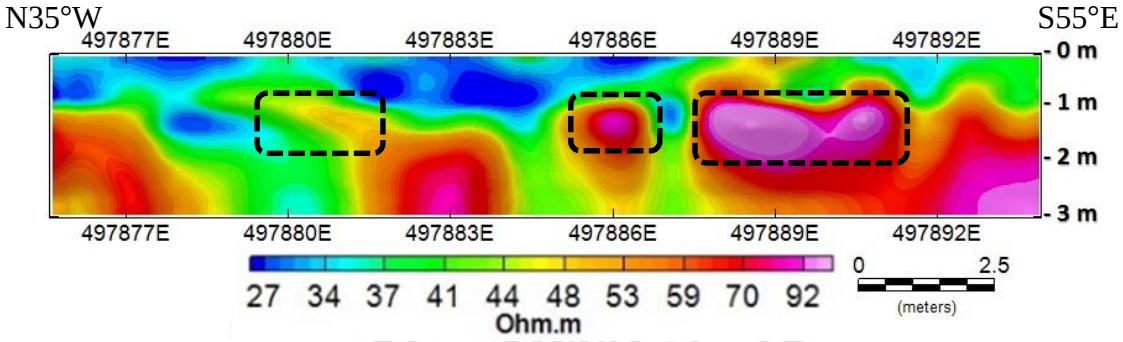

Figure 3.23 3D Inversion model of vertical slices of Area 1, Section 4 (The black rectangles present high resistivity anomaly zones).

The results of the 3D inversion model of Area 1 (Figure 3.24) shown in X-Z plane, Section 5. The anomalies of interest were in the black rectangles.

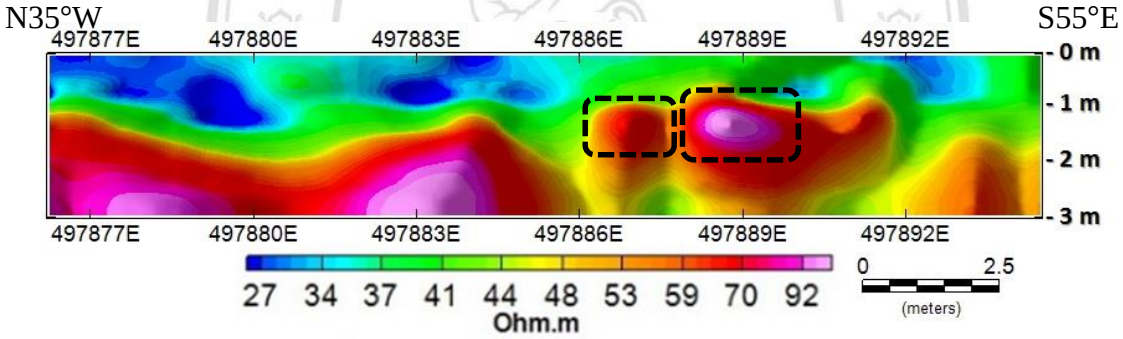

Figure 3.24 3D Inversion model of vertical slices of Area 1, Section 5 (The black rectangles present high resistivity anomaly zones).

The results of the 3D inversion model of Area 1 (Figure 3.25) shown in X-Z plane, Section 6. The anomaly of interest was in the black rectangle.

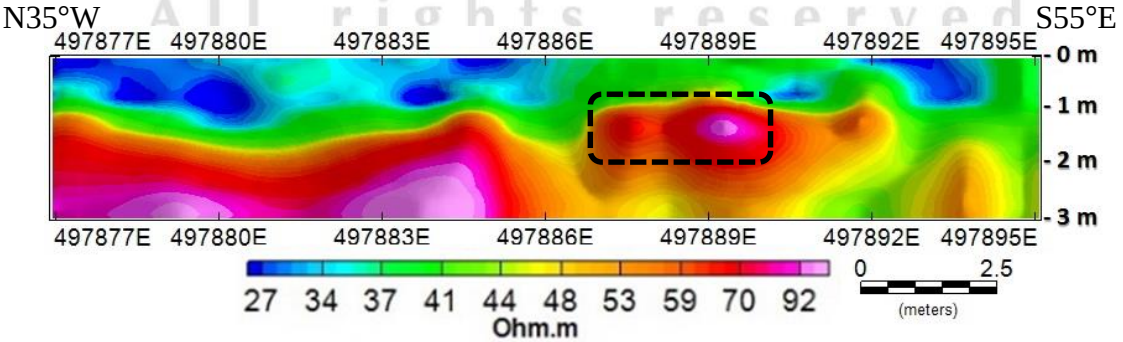

Figure 3.25 3D Inversion model of vertical slices of Area 1, Section 6 (The black rectangles present high resistivity anomaly zones).

Area 2

The data inversion obtained vertical slices (sections) for X-Z plane of Area 2 (Figure 3.26). The results show interesting trends of anomaly at the top and bottom of each section. The anomalies of interest had an apparent resistivity over 200 Ohm.m, a dimension of 2x3 m, and the thicknesses of anomalies were 1-1.5 m with a contiguous section.

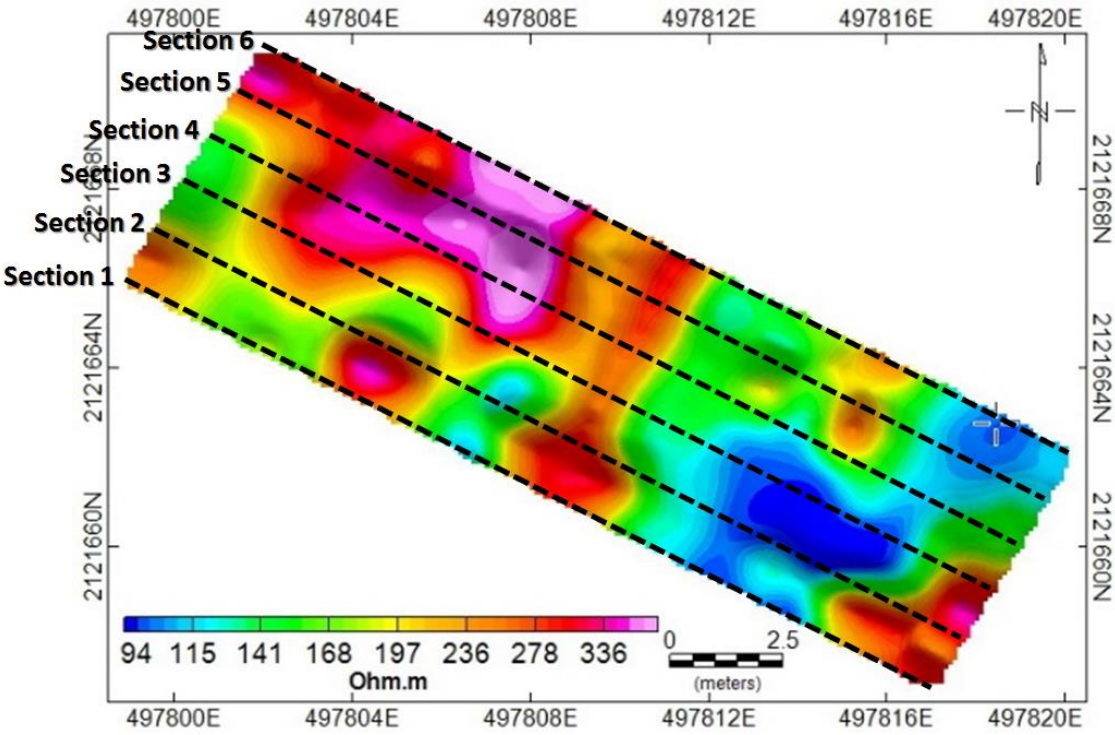

Figure 3.26 Map showing line sections of Area 2 (Dash lines are study line).

The results of the 3D inversion model of Area 2 (Figure 3.27) shown in X-Z plane, Section 1. The anomalies of interest were in the black rectangles.

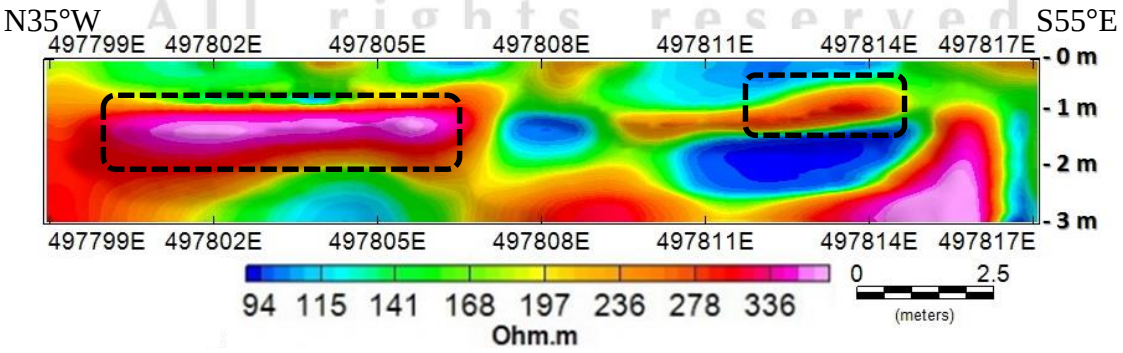

Figure 3.27 3D Inversion model of vertical slices of Area 2, Section 1 (The black rectangles present high resistivity anomaly zones).

The results of the 3D inversion model of Area 2 (Figure 3.28) shown in X-Z plane, Section 2. The anomalies of interest were in the black rectangles.

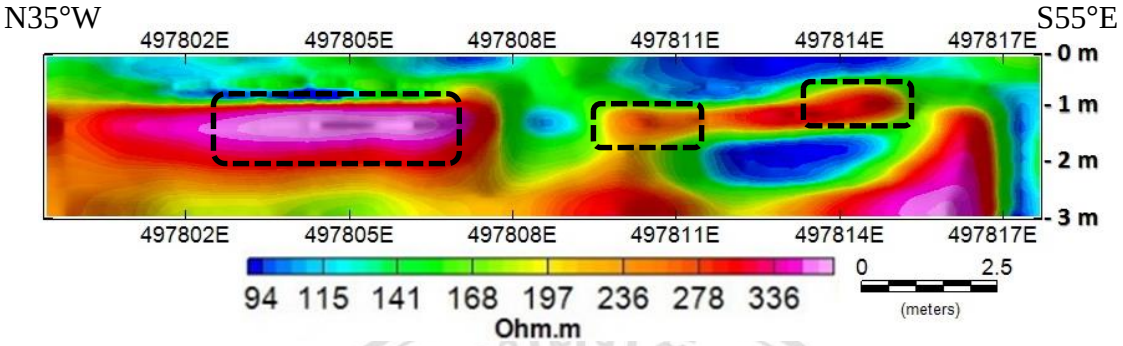

Figure 3.28 3D Inversion model of vertical slices of Area 2, Section 2 (The black rectangles present high resistivity anomaly zones).

The results of the 3D inversion model of Area 2 (Figure 3.29) shown in X-Z plane, Section 3. The anomalies of interest were in the black rectangles.

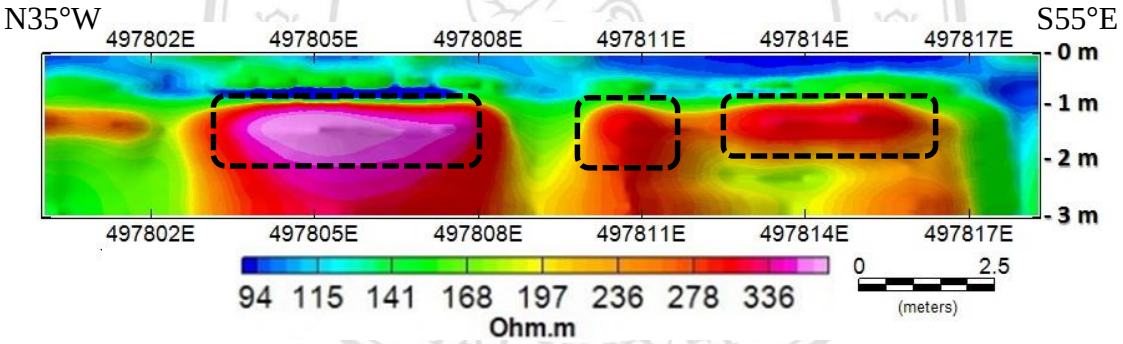

Figure 3.29 3D Inversion model of vertical slices of Area 2, Section 3 (The black rectangles present high resistivity anomaly zones).

The results of the 3D inversion model of Area 2 (Figure 3.30) shown in X-Z plane, Section 4. The anomalies of interest were in the black rectangles.

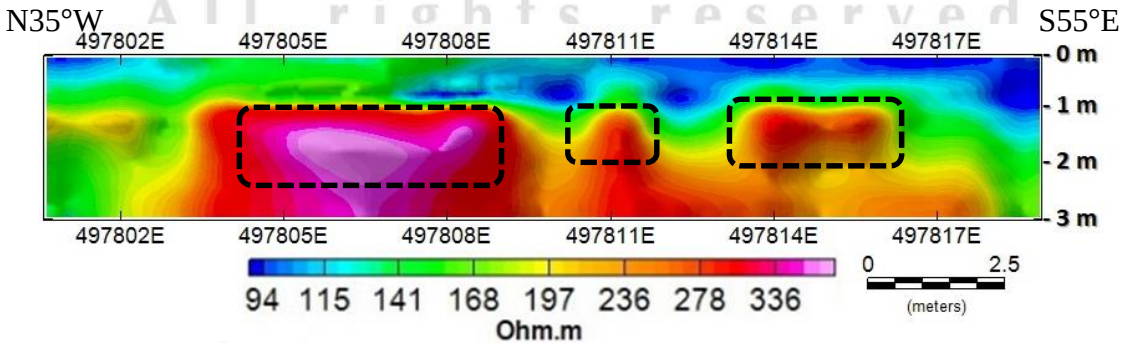

Figure 3.30 3D Inversion model of vertical slices of Area 2, Section 4 (The black rectangles present high resistivity anomaly zones).

The results of the 3D inversion model of Area 2 (Figure 3.31) shown in X-Z plane, Section 5. The anomalies of interest were in the black rectangles.

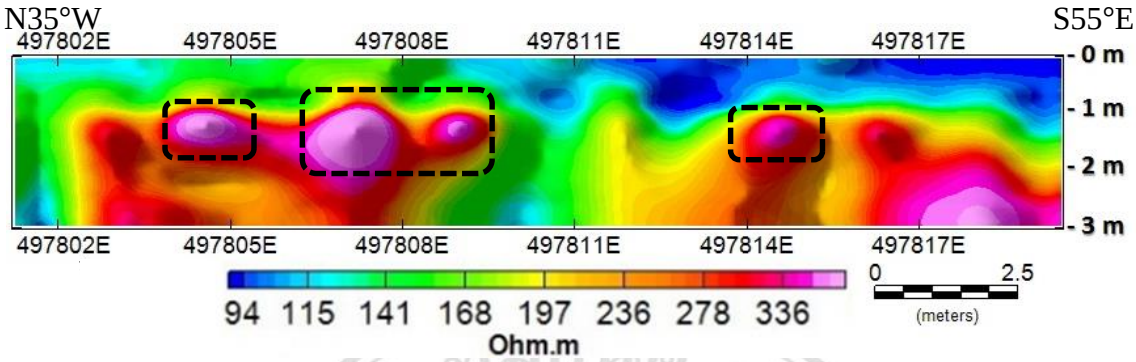

Figure 3.31 3D Inversion model of vertical slices of Area 2, Section 5 (The black rectangles present high resistivity anomaly zones).

The results of the 3D inversion model of Area 2 (Figure 3.32) shown in X-Z plane, Section 6. The anomalies of interest were in the black rectangles.

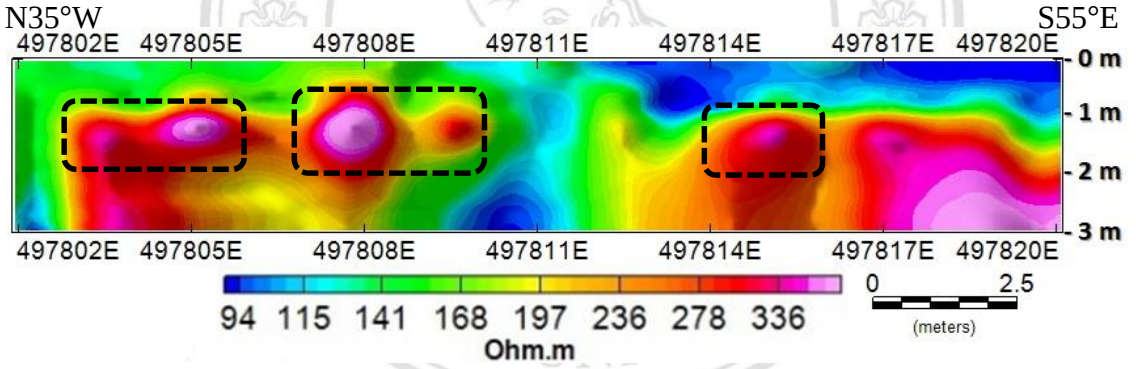

Figure 3.32 3D Inversion model of vertical slices of Area 2, Section 6 (The black rectangles present high resistivity anomaly zones).